Microwave Spectroscopy of a Single Permalloy Chiral Metamolecule on a Coplanar Waveguide

Toshiyuki Kodama,[1] Yusaku Kusanagi,[2] Satoshi Okamoto,[2] Nobuaki Kikuchi,[2] Osamu Kitakami,[2] Satoshi Tomita,[1,*] Nobuyoshi Hosoito,[1] and Hisao Yanagi[1]

[1]*Graduate School of Materials Science, Nara Institute of Science and Technology, Ikoma, Nara 630-0192, Japan*

[2]*Institute of Multidisciplinary Research for Advanced Materials, Tohoku University, Sendai, Miyagi 980-8577, Japan*

(Received 4 April 2017; revised manuscript received 8 February 2018; published 17 May 2018)

We investigate the microwave spectroscopies of a micrometer-sized single permalloy (Py) chiral structure on coplanar waveguides (CPWs). Under an external dc magnetic field applied in a direction perpendicular to the microwave propagation, the Py chiral structure loaded on the center of the CPW signal line shows Kittel-mode ferromagnetic resonance. Contrastingly, the structure on the signal-line edge highlights two additional resonances: spin-wave resonance at a higher frequency, and unique resonance at a lower frequency of approximately 7.8 GHz. The resonance signal at 7.8 GHz originates from magnetically induced, geometry-driven resonance, although the resonance frequency does not depend on the external magnetic field. Moreover, the displacement of the Py structures on the signal line results in nonreciprocal microwave transmission, which is traced back to the edge-guide mode.

DOI: 10.1103/PhysRevApplied.9.054025

I. INTRODUCTION

Electromagnetic metamaterials are artificial structures comprising subwavelength-sized units, called meta-atoms or metamolecules. Control of interactions among well-designed meta-atoms or metamolecules in metamaterials enables the realization of intriguing properties not typically observed in nature [1]; for example, negative refractive index [2,3], cloaking [4], and narrow-band perfect absorption [5]. Since the metamaterials' properties primary originate from functions of the meta-atoms or metamolecules, investigations of the single meta-atom or metamolecule is of great importance. Similar issues are found in research on nanostructured materials comprising nanoparticles. Properties of nanostructured materials show inhomogeneous broadening caused by a distribution in nanoparticle size and properties. Single-particle spectroscopy is thus a powerful technique for eliminating the inhomogeneous broadening [6]. This concept is imported into metamaterials research in this paper by performing a microwave spectroscopy of a single metamolecule. This single-metamolecule spectroscopy leads to high-throughput developments in metamaterial engineering.

Here, we focus on micrometer-sized permalloy ($Fe_{21.5}Ni_{78.5}$, Py) chiral structures—Py chiral metamolecules [7,8]. In our previous report [8], Py chiral metamolecules were fabricated using strain-driven self-coiling [9,10]. Ferromagnetic resonance (FMR) was studied using a cavity and a coplanar waveguide (CPW). In CPW FMR, microwave transmission was measured as a function of frequency for a single Py chiral metamolecule under a dc magnetic field, bringing about magnetic material parameters [e.g., effective g value (g_{eff}), saturation magnetization ($\mu_0 M_{\mathrm{eff}}$), and Gilbert damping factor] of the single metamolecule. However, detailed spectroscopic studies of the single metamolecule on a CPW remain unexplored.

In this work, the microwave transmission spectra of the single Py metamolecule are measured by changing the metamolecule's position on the CPW. The Py chiral metamolecule loaded on the CPW signal-line center shows Kittel-mode FMR, whereas the metamolecule at the edge highlights additional two resonances besides the Kittel-mode FMR: spin-wave resonance due to localized resonance modes at a higher frequency and magnetically induced, geometry-driven resonance at a lower frequency of approximately 7.8 GHz. Furthermore, the displacement of the Py structure results in a nonreciprocal microwave transmission, which is traced back to the edge-guide mode, at the FMR frequency.

II. EXPERIMENTAL PROCEDURES

The Py chiral metamolecules are fabricated using a strain-driven self-coiling technique [9]. Strips of SU8 resin are patterned on a Si substrate. The strip thickness, width, and length are 8 μm, 9 μm, and 1.1 mm, respectively.

*tomita@ms.naist.jp

A 60-nm-thick Py film is deposited on the SU8 strips. The strips with the Py film on the top are peeled from the substrate by dipping into *N*-methyl-2-pyrrolidone (NMP) and coiled spontaneously owing to the strain in the bilayer.

A drop of NMP containing a single Py metamolecle is pipetted and transferred to a CPW patterned by gold (Au) on a quartz substrate using standard photolithography. The CPW comprises three Au lines: one signal line (S) sandwiched between two ground lines (Gs), as depicted in Fig. 1. The signal-line width and length are 82 μm and 1 mm, respectively. The gap between the S and the G is 9 μm. After drying the NMP in air, we obtain a single Py metamolecule loaded on the CPW signal line. The CPW is connected to a vector network analyzer (VNA; Agilent E8363C) via three terminal probes.

The cross section of the Py metamolecule loaded on the CPW is illustrated in Fig. 1. The Py metamolecule chiral axis is parallel to the z axis, which is perpendicular to microwave propagation (the x axis). The inner plane of the metamolecule is Py, while the outer one is SU8. The displacement of the metamolecule position on the signal line is represented by d, which is the distance between the signal-line center and the chiral axis. When the microwave propagation is observed from port 1, as shown in Fig. 1, the positive value of d corresponds to the displacement of the metamolecule on the right-hand side on the signal line, while a negative d value corresponds to the displacement on the left-hand side on the signal line. An external dc magnetic field ($H_{\rm ext}$) is applied by an electromagnet in the z direction, which is parallel to the chiral axis and the Py film plane in the metamolecule, as shown in Fig. 1.

The microwaves propagating in the signal line generate ac magnetic fields ($H_{\rm ac}$). The $H_{\rm ac}$ for driving FMR is in the y direction at the signal-line center, whereas the $H_{\rm ac}$ is in the z direction at the gap between S and G. We measure microwave transmission thorough the signal line at room temperature. The microwave transmission coefficient from port 1 to port 2 (from port 2 to port 1) is assigned to the S parameter of S_{21} (S_{12}). S_{21} and S_{12} can be obtained simultaneously using a VNA with a frequency sweep of 1–40 GHz.

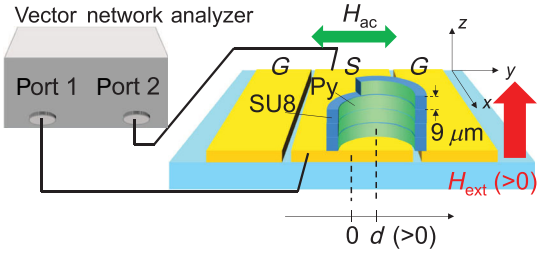

FIG. 1. Cross-section illustration of the CPW and the Py chiral metamolecule. The width of the center signal line (S) is 82 μm and the gap between the signal and ground (G) lines is 9 μm. The position of the metamolecule on the signal line is defined by the distance d between the signal-line center and the chiral axis.

III. RESULTS AND DISCUSSION

A. CPW FMR of a single Py chiral metamolecule

FMR driven by $H_{\rm ac}$ gives rise to the absorption of propagating microwaves [11]. The FMR signal is observed as a dip in the S_{21} (S_{12}) spectra [12–14]. However, the FMR signal from the single metamolecule is quite small. In order to highlight the FMR signal, we derive $\Delta|S_{21}|$ as

$$\Delta|S_{21}| = |S_{21}^{\rm raw}| - |S_{21}^{\rm bg}|, \tag{1}$$

where $S_{21}^{\rm raw}$ corresponds to S_{21} under a specific nonzero magnetic field and $S_{21}^{\rm bg}$ to S_{21} under a zero magnetic field. $S_{21}^{\rm bg}$ is measured just before every measurement of $S_{21}^{\rm raw}$. $\Delta|S_{12}|$ is obtained in a similar way.

Figure 2(a) shows the optical microscope image of the metamolecule placed on the signal-line center ($d = 0$ μm). The CPW signal line is highlighted in yellow for better visibility. The metamolecule diameter is about 60 μm [8]. The $\Delta|S_{21}|$ spectra at various $\mu_0 H_{\rm ext}$ values are illustrated in Fig. 2(b). The dip observed at 8.41 GHz under $\mu_0 H_{\rm ext} =$ 100 mT shifts to 32.7 GHz under $\mu_0 H_{\rm ext} = 800$ mT [8]. Figure 2(c) shows the directional difference in microwave transmission, $\Delta|S_{21}| - \Delta|S_{12}|$, of the metamolecule on the signal-line center ($d = 0$ μm). In Fig. 2(c), the $\Delta|S_{21}| - \Delta|S_{12}|$ spectra at various $\mu_0 H_{\rm ext}$ values are vertically aligned for better visibility. While small fringes are seen at a higher frequency, $\Delta|S_{21}|$ and $\Delta|S_{12}|$ are very similar,

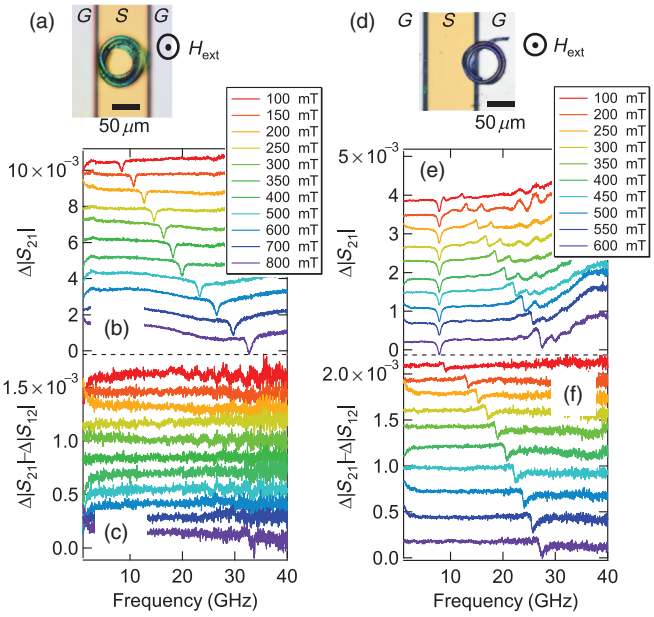

FIG. 2. Optical microscope images of a Py chiral metamolecule with (a) $d = 0$ μm and (d) $d = 60$ μm. Signal lines of CPW are highlighted in yellow. (b),(e) Corresponding microwave transmission spectra $\Delta|S_{21}|$ at various external magnetic fields ($\mu_0 H_{\rm ext}$). (c) and (f) are the corresponding directional differential spectra $\Delta|S_{21}| - \Delta|S_{12}|$. (a) and (b) are reproduced from Ref. [8].

indicating no nonreciprocity in the $\Delta|S_{21}| - \Delta|S_{12}|$ spectra. $\Delta|S_{21}|$ and $\Delta|S_{12}|$ do not present the same magnitude at a very low frequency of approximately 5 GHz. However, the difference is very small and the contribution from the background signal fluctuation cannot be ruled out.

The optical microscope image of the metamolecule placed at the signal-line edge ($d = 60$ μm) is shown in Fig. 2(d). Figure 2(e) illustrates the $\Delta|S_{21}|$ spectra in this configuration. In contrast to the solo resonance signal by the Py metamolecule in Fig. 2(b), three resonance signals are observed in Fig. 2(e): the first at 7.80 GHz, the second at 8.68 GHz, and the third at 12.1 GHz under $\mu_0 H_{\rm ext} =$ 100 mT. As $\mu_0 H_{\rm ext}$ increases, the second and third resonance signals shift to higher frequencies and arrive, finally, at around 26.5 and 29.3 GHz, with $\mu_0 H_{\rm ext} = 600$ mT. Contrastingly, the first resonance dip, observed at 7.80 GHz with $\mu_0 H_{\rm ext} = 100$ mT, does not move with an increase in $\mu_0 H_{\rm ext}$. These three resonances are observed also in reflection $\Delta|S_{11}|$ spectra for a metamolecule placed at the signal-line edge, as illustrated in the Supplemental Material [15]. Figure 2(f), $\Delta|S_{21}| - \Delta|S_{12}|$ spectra of the metamolecule at the signal-line edge ($d = 60$ μm), highlights the emergence of a nonreciprocal resonance signal at the second resonance frequency. The nonreciprocity signal has a dispersion-type shape. Note that the nonreciprocity signal is not caused by the magnetochiral effects observed in Refs. [16–18] because $H_{\rm ext}$ is applied in the direction perpendicular to the microwave propagation.

B. Origins of resonances

In Fig. 3(a), frequencies of the dip observed in Fig. 2(b) for the Py chiral metamolecule at the signal-line center ($d = 0$ μm) are plotted as a function of $\mu_0 H_{\rm ext}$ (the black open circles). The most likely origin of the dip is the Kittel-mode FMR corresponding to uniform precession of electron spins in Py films [19]. The solid line in Fig. 3(a) is thus a fitting curve using the Kittel formula [20] for a magnetic film with $H_{\rm ext}$ applied in the direction parallel to the film plane. The fitting procedure results in a $g_{\rm eff}$ value of 2.1590 ± 0.0082 and a $\mu_0 M_{\rm eff}$ value of 681.77 ± 9.01 mT [8]. The $\mu_0 M_{\rm eff}$ value of the Py chiral metamolecule is smaller than that of the metallic Py thin film (1.05 T) given in the literature [21]. The small $\mu_0 M_{\rm eff}$ value indicates surface and interface anisotropies due to unsaturated spins [22] in the Py films on the SU8 film for the Py metamolecule [8]. Since these fitting parameters are reasonable values, the dip is caused by the Kittel-mode FMR in the Py thin film of the metamolecule.

The blue crosses in Fig. 3(a) correspond to resonance frequencies of the chiral metamolecule at the edge ($d = 60$ μm) observed in Fig. 2(e). Figure 3(a) clearly shows that the frequency of the first resonance is independent of $\mu_0 H_{\rm ext}$. Contrastingly, the frequencies of the second and third resonances shift to higher frequencies as $\mu_0 H_{\rm ext}$ increases. The second resonance frequency agrees

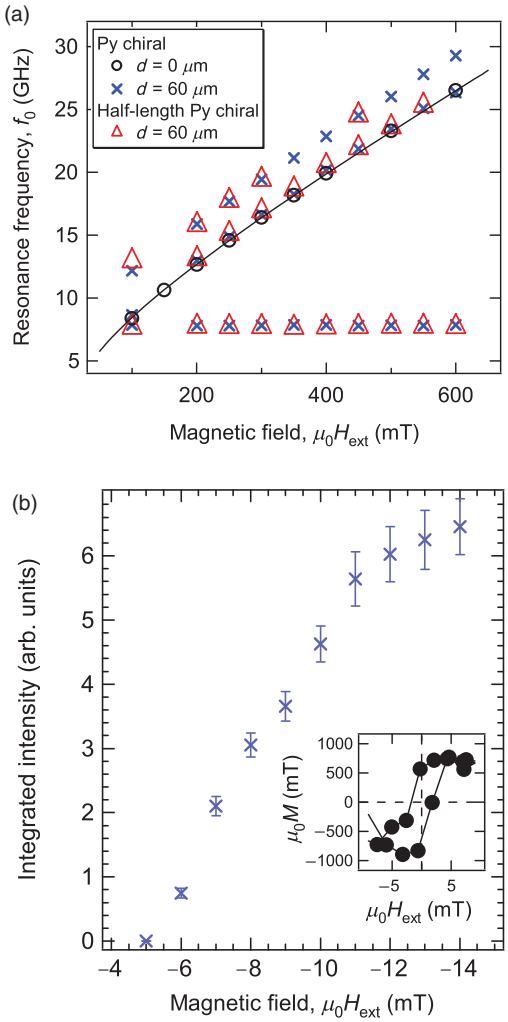

FIG. 3. (a) Resonance frequencies are plotted as a function of $\mu_0 H_{\rm ext}$. Black open circles and blue crosses correspond, respectively, to resonance frequencies observed for Py metamolecules with $d = 0$ [in Fig. 2(b)] and 60 μm [in Fig. 2(e)]. Red open triangles correspond to the results for a Py metamolecule consisting of a half-length Py strip. The solid line indicates a theoretical curve fitted by the Kittel formula. (b) Integrated intensity of a metamolecule's 7.8-GHz resonance (blue crosses) are plotted as a function of $\mu_0 H_{\rm ext}$. (Inset) In-plane magnetization ($\mu_0 M$) hysteresis loop of a Py thin film (the black solid circles).

well with the $\mu_0 H_{\rm ext}$ dependence of the Kittel-mode FMR, as indicated by the solid line. The third resonance signal, at a higher frequency than the Kittel mode, is likely to be caused by spin-wave resonance with a nonzero wave number [19].

It has been reported that tubular magnetic structures [23,24] show resonance signals due to the constructive interference of Damon-Eshbach–type spin waves [25], which are traveling along the circumference of the tube. This mode is very similar to acoustic [26] and optical [27] whispering gallery modes (WGMs). However, highly symmetric WGMs are an unlikely starting point for this work. If the WGMs were the origin, the Py metamolecule

on the signal-line center (the black open circles) would show spin-wave resonance. While ac magnetic fields are parallel to the y axis at the signal-line center, those at the edge of the CPW signal line have a z-direction component parallel to the chiral axis. In this way, the spin-wave resonance signals accompanied by the Kittel mode FMR observed in the metamolecule are traced back to the localized resonance modes due to the inhomogeneous ac fields [8,28].

In general, the frequency of magnetic resonances, for example, Kittel-mode FMR and spin-wave resonance, is proportional to $\mu_0 H_{\rm ext}$. Nevertheless, Fig. 3(a) demonstrates that the first resonance frequency of 7.8 GHz (the blue crosses) is independent of $\mu_0 H_{\rm ext}$. Therefore, one may consider that the origin of the resonance at 7.8 GHz is not magnetically induced resonance but antenna resonance. However, this is not true. In the following, we show that the resonance at 7.8 GHz is induced magnetically.

We prepare a control chiral structure using a Py strip length of 0.5 mm, which is almost half the length of the original Py strips in the metamolecule. The half-length metamolecule is placed at the signal-line edge and studied by CPW FMR. An optical microscopic image and CPW-FMR spectra for the half-length metamolecule are shown in the Supplemental Material [15]. The short chiral metamolecule demonstrates three resonance signals. The resonance frequencies are plotted as a function of $\mu_0 H_{\rm ext}$ in Fig. 3(a) as red open triangles. The red open triangles agree well with the blue crosses of the original metamolecule with 1.1-mm-long Py strip at the signal-line edge. In particular, the first resonance frequency is identical at 7.8 GHz in both samples. Therefore, antenna resonance is ruled out as the origin of the resonance signal at 7.8 GHz [15]. Additionally, we have measured 1.1-mm-long chiral structures with different diameters, as shown in the Supplemental Material [15]. Identical 7.8-GHz resonances, whose frequencies are independent of $\mu_0 H_{\rm ext}$, are observed for chiral metamolecules with different lengths and diameters. The identical resonance frequencies indicate a constant effective magnetic field in the Py chiral metamolecule.

Figure 3(b) presents additional evidence that the first resonance is magnetically induced. As shown by the blue crosses in Fig. 3(b), the integrated intensity of the 7.8-GHz resonance signal from the metamolecule at the line edge is plotted as a function of a very small $\mu_0 H_{\rm ext}$ value of -5 to -14 mT. Because a remanent magnetic field of the electromagnet used in the CPW-FMR measurements is -5 mT, the intensity is evaluated by fitting the spectra using the Lorentz function and normalized by the signal intensity with $\mu_0 H_{\rm ext} = -5$ mT. The integrated signal intensity of the first resonance increases as the absolute value of $\mu_0 H_{\rm ext}$ increases.

In the inset of Fig. 3(b), the black solid circles correspond to a in-plane magnetization hysteresis loop ($\mu_0 M$ vs $\mu_0 H_{\rm ext}$) measured with a vibrating-sample magnetometer of a 60-nm-thick Py film deposited on a substrate using the sputtering technique. Here, we use a magnetization curve of the Py film, not the Py metamolecule, because the Py metamolecule's magnetization is too tiny to be measured with the magnetometer. Although a magnetization curve of ten Py metamolecules is measured with an alternating-gradient magnetometer in our previous work [8], the magnetization at approximately zero field is not reliable. In Fig. 3(b), the evolution of the integrated intensity of the first resonance signal is very similar to that of the Py film magnetization, but different from the intensity evolution of the Kittel-mode resonance, as shown in the Supplemental Material [15].

C. CPW FMR of the control Py rings

Given that the ac magnetic field penetrates into the chiral structure, LC resonance which is very similar to that in a split-ring resonator [1] is plausible. However, five control Py rings at the CPW signal edge highlight only the Kittel-mode FMR, as shown in Fig. 4. Figures 4(a) and 4(d), respectively, show photographs of the control Py ring sample with $d = 0$ and -20 μm patterned on the CPW using the photolithography and lift-off processes. The inner and outer diameters of the ring are 60 and 80 μm, similar to the diameter of the Py chiral metamolecule. The Py film thickness is 60 nm. For insulating between the signal and ground lines, a thin SiO_2 layer is deposited underneath the

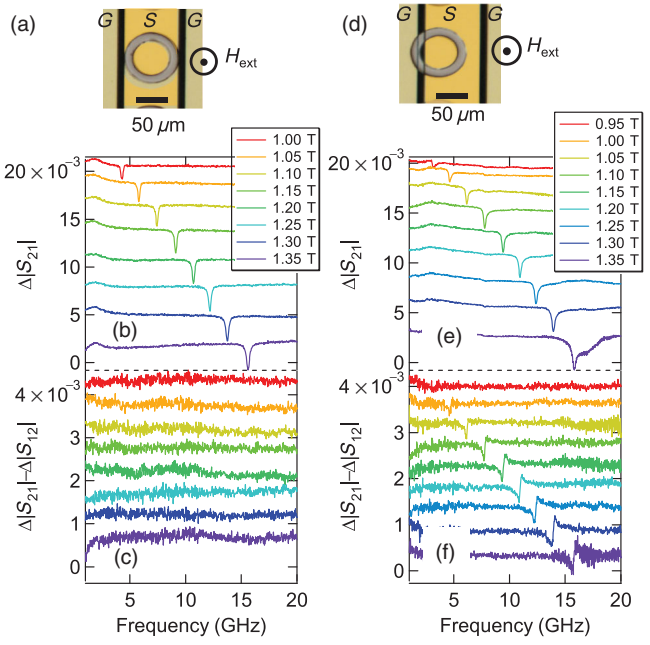

FIG. 4. Optical microscope images of Py rings with (a) $d = 0$ μm and (d) $d = -20$ μm. Signal lines of the CPW are highlighted in yellow. (b) and (e) are, respectively, $\Delta|S_{21}|$ spectra of Py rings with $d = 0$ μm and $d = -20$ μm at various $\mu_0 H_{\rm ext}$ values. (c),(f) Corresponding directional differential spectra $\Delta|S_{21}| - \Delta|S_{12}|$.

Py rings. H_{ext} is applied in the direction perpendicular to the CPW planes.

The $\Delta|S_{21}|$ spectra of the Py rings with $d = 0$ and $d = -20$ μm for various $\mu_0 H_{ext}$ values are shown in Figs. 4(b) and 4(e), respectively. In both samples, we observe a solo resonance dip at approximately 4 GHz when $\mu_0 H_{ext} = 1$ T and a blueshift of the dip with an increase in $\mu_0 H_{ext}$. The resonances observed for the Py rings are traced back to the Kittel mode, although the resonance field is much higher than that for chiral metamolecules owing to the large demagnetization field in the Py film perpendicular to the magnetic fields. Figures 4(c) and 4(f) illustrate the $\Delta|S_{21}| - \Delta|S_{12}|$ spectra of the Py rings on the signal-line center and edge, respectively. Figure 4(f) shows nonreciprocal signals, while Fig. 4(c) shows no signals. The dispersion-type shape of the nonreciprocal signal in Fig. 4(f) is inverted compared to that in Fig. 2(f). Although the signal shape is inverted, the directional nonreciprocity signal is observed in both the Py chiral metamolecule and the Py rings only on the signal-line edge. In this way, we conclude that, at the signal-line edge, three-dimensional (3D) and two-dimensional magnetic structures cause the nonreciprocity signal at the Kittel-mode resonance frequency. Moreover, the tubularlike 3D structures at the signal-line edge give rise to the magnetically induced, but magnetic-field-independent, resonance at 7.8 GHz.

A nonreciprocal propagation of microwaves has been reported in asymmetrically deposited magnetic materials on CPWs. The nonreciprocity measured in this paper is traced back to the edge-guide mode [29]. Magnetic nanowires placed at the gap between the signal and ground lines of the CPW [30] and nanowires with different heights underneath the CPW [31] show a nonreciprocal transmission. The nonreciprocal transmission is very similar to that in the signal line, with stubs on the one edge [32]. In this work, when the Py metamolecule and ring are loaded on the signal-line edge, the Py structure is asymmetric on the signal line. Therefore, microwaves propagating from port 1 to port 2, and from port 2 to port 1, feel the different volumes of Py. As a result, the FMR intensity differs between the $\Delta|S_{21}|$ and $\Delta|S_{12}|$, resulting in the nonreciprocal resonance signal.

IV. CONCLUSION

In conclusion, a single metamolecule spectroscopy is conducted in this paper at microwave frequencies using a CPW and a VNA. Our measurements of the Py chiral metamolecule loaded on the signal-line center demonstrate Kittel-mode FMR. Contrastingly, the Py metamolecules loaded on the signal-line edge show two additional magnetic resonances besides the Kittel-mode FMR. A high-frequency resonance accompanied by the Kittel-mode FMR is spin-wave resonance. Though another resonance at a lower frequency of approximately 7.8 GHz is independent of the dc magnetic field, this resonance is also a magnetically induced resonance. In addition, a nonreciprocal resonance signal at the Kittel-mode FMR frequency is highlighted for the Py chiral metamolecule, as well as for the Py rings at the signal-line edge. This nonreciprocity is traced back to the edge-guide mode using asymmetrical Py deposition on the signal line.

ACKNOWLEDGMENTS

This work was supported by Japan Society for the Promotion of Science (JSPS) KAKENHI (Grants No. 26287065 and No. 16K04881). The CPW-FMR work was performed under the Cooperative Research Program "Network Joint Research Center for Materials and Devices." T. K. acknowledges support from a Grant-in-Aid coming from a JSPS Research Fellowship.

[1] D. R. Smith, J. B. Pendry, and M. C. K. Wiltshire, Metamaterials and negative refractive index, Science **305**, 788 (2004).

[2] V. G. Veselago, The electrodynamics of substances with simultaneously negative values of ϵ and μ, Sov. Phys. Usp. **10**, 509 (1968).

[3] J. B. Pendry, Negative Refraction Makes a Perfect Lens, Phys. Rev. Lett. **85**, 3966 (2000).

[4] D. Schurig, J. J. Mock, B. J. Justice, S. A. Cummer, J. B. Pendry, A. F. Starr, and D. R. Smith, Metamaterial electromagnetic cloak at microwave frequencies, Science **314**, 977 (2006).

[5] X. Liu, T. Tyler, T. Starr, A. F. Starr, N. M. Jokerst, and W. J. Padilla, Taming the Blackbody with Infrared Metamaterials as Selective Thermal Emitters, Phys. Rev. Lett. **107**, 045901 (2011).

[6] S. Nie and S. R. Emory, Probing single molecules and single nanoparticles by surface-enhanced Raman scattering, Science **275**, 1102 (1997).

[7] T. Kodama, S. Tomita, N. Hosoito, and H. Yanagi, Fabrication and ferromagnetic resonance of cobalt chiral metamolecule arrays, Appl. Phys. A **122**, 41 (2016).

[8] T. Kodama, S. Tomita, T. Kato, D. Oshima, S. Iwata, S. Okamoto, N. Kikuchi, O. Kitakami, N. Hosoito, and H. Yanagi, Ferromagnetic Resonance of a Single Magneto-chiral Metamolecule of Permalloy, Phys. Rev. Applied **6**, 024016 (2016).

[9] E. J. Smith, D. Makarov, S. Sanchez, V. M. Fomin, and O. G. Schmidt, Magnetic Microhelix Coil Structures, Phys. Rev. Lett. **107**, 097204 (2011).

[10] R. Streubel, P. Fischer, F. Kronast, V. P. Kravchuk, D. D. Sheka, Y. Gaididei, O. G. Schmidt, and D. Makarov, Magnetism in curved geometries, J. Phys. D **49**, 363001 (2016).

[11] N. Kikuchi, Y. Suyama, S. Okamoto, O. Kitakami, and T. Shimatsu, Quasi-ballistic magnetization switching in Co/Pt dots with perpendicular magnetization, Appl. Phys. Lett. **104**, 112409 (2014).

[12] Y. Ding, T. J. Klemmer, and T. M. Crawford, A coplanar waveguide permeameter for studying high-frequency properties of soft magnetic materials, J. Appl. Phys. **96**, 2969 (2004).

[13] D. Pain, M. Ledieu, O. Acher, A. L. Adenot, and F. Duverger, An improved permeameter for thin film measurements up to 6 GHz, J. Appl. Phys. **85**, 5151 (1999).
[14] G. Counil, J.-V. Kim, T. Devolder, C. Chappert, K. Shigeto, and Y. Otani, Spin wave contributions to the high-frequency magnetic response of thin films obtained with inductive methods, J. Appl. Phys. **95**, 5646 (2004).
[15] See Supplemental Material at http://link.aps.org/supplemental/10.1103/PhysRevApplied.9.054025 for reflection $\Delta|S_{11}|$ spectra corresponding to Figs. 2(b) and 2(e), an optical microscopic image and CPW-FMR spectra for metamolecules with different lengths and diameters placed at the signal-line edge, the origin of the resonance signal at 7.8 GHz, and the intensity evolution of the Kittel-mode resonance.
[16] S. Tomita, K. Sawada, A. Porokhnyuk, and T. Ueda, Direct Observation of Magnetochiral Effects through a Single Metamolecule in Microwave Regions, Phys. Rev. Lett. **113**, 235501 (2014).
[17] S. Tomita, H. Kurosawa, K. Sawada, and T. Ueda, Enhanced magnetochiral effects at microwave frequencies by a single metamolecule, Phys. Rev. B **95**, 085402 (2017).
[18] S. Tomita, H. Kurosawa, T. Ueda, and K. Sawada, Metamaterials with magnetism and chirality, J. Phys. D **51**, 083001 (2018).
[19] C. Kittel, *Introduction to Solid State Physics*, 7th ed. (Wiley, New York, 1995).
[20] Y. Ajiro, H. Yazawa, K. Kawaguchi, N. Hosoito, and T. Shinjo, Ferromagnetic resonance of Fe/Mg multilayered films with artificial superstructure, J. Phys. Soc. Jpn. **58**, 3339 (1989).
[21] J. P. Nibarger, R. Lopusnik, Z. Celinski, and T. J. Silva, Variation of magnetization and the Landé g factor with thickness in Ni-Fe films, Appl. Phys. Lett. **83**, 93 (2003).
[22] J. M. Shaw, H. T. Nembach, and T. J. Silva, Determination of spin pumping as a source of linewidth in sputtered $Co_{90}Fe_{10}$/Pd multilayers by use of broadband ferromagnetic resonance spectroscopy, Phys. Rev. B **85**, 054412 (2012).
[23] S. Mendach, J. Podbielski, J. Topp, W. Hansen, and D. Heitmann, Spin-wave confinement in rolled-up ferromagnetic tubes, Appl. Phys. Lett. **93**, 262501 (2008).
[24] F. Balhorn, S. Mansfeld, A. Krohn, J. Topp, W. Hansen, D. Heitmann, and S. Mendach, Spin-Wave Interference in Three-Dimensional Rolled-Up Ferromagnetic Microtubes, Phys. Rev. Lett. **104**, 037205 (2010).
[25] R. W. Damon and J. R. Eshbach, Magnetostatic modes of a ferromagnet slab, J. Phys. Chem. Solids **19**, 308 (1961).
[26] L. Rayleigh, The problem of the whispering gallery, Philos. Mag. **20**, 1001 (1910).
[27] K. J. Vahala, Optical microcavities, Nature (London) **424**, 839 (2003).
[28] F. Giesen, J. Podbielski, and D. Grundler, Mode localization transition in ferromagnetic microscopic rings, Phys. Rev. B **76**, 014431 (2007).
[29] M. E. Hines, Reciprocal and nonreciprocal modes of propagation in ferrite stripline and microstrip devices, IEEE Trans. Microwave Theory Tech. **19**, 442 (1971).
[30] B. K. Kuanr, V. Veerakumar, R. Marson, S. R. Mishra, R. E. Camley, and Z. Celinski, Nonreciprocal microwave devices based on magnetic nanowires, Appl. Phys. Lett. **94**, 202505 (2009).
[31] J. De La Torre Medina, J. Spiegel, M. Darques, L. Piraux, and I. Huynen, Differential phase shift in nonreciprocal microstrip lines on magnetic nanowired substrates, Appl. Phys. Lett. **96**, 072508 (2010).
[32] T. Ueda and M. Akiyama, Nonreciprocal phase-shift composite right/left handed microstrip lines using ferrite-rod-embedded substrate, IEEE Trans. Magn. **45**, 4203 (2009).